International Journal of Microwave and Wireless Technologies

cambridge.org/mrf

Slotted vertical wall for decoupling and beam tilt correction

Yiying Wang[1], Shengfei Zhang[1], Bo Wang[2], Hongxin Zhang[3], Yannan Jiang[1], Wanghua Pan[1] and Ahmed A. Kishk[4]

[1]Guangxi Key Lab of Wireless Wideband Communication and Signal Processing, Guilin University of Electronic Technology, Guilin, Guangxi, China; [2]Xi'an Electronic Engineering Research Institute, Xi'an, Shanxi, China; [3]Beijing University of Posts and Telecommunications, Beijing, China and [4]Department of Electrical and Computer Engineering, Concordia University, Montreal, QC, Canada

Research Paper

Cite this article: Wang Y, Zhang S, Wang B, Zhang H, Jiang Y, Pan W, Kishk AA (2024) Slotted vertical wall for decoupling and beam tilt correction. *International Journal of Microwave and Wireless Technologies* **16**(1), 162–166. https://doi.org/10.1017/S1759078723000752

Received: 08 November 2022
Revised: 27 May 2023
Accepted: 30 May 2023

Keywords:
close spacing; decoupling; patch antenna; pattern correction; vertical wall

Corresponding author: Wanghua Pan; Email: pwh2008_79@163.com

Abstract

An intra-band pattern-corrected decoupling vertical conducting wall is realized by dielectric substrate with conductor cladding on both side wall between two tightly spaced H-plane microstrip patches with $\lambda_0/20$ edge-to-edge spacing. The wall is grounded and two symmetrical slots are etched on the vertical substrate. The measured results agree with the simulations, showing that the slotted vertical wall reduces the mutual coupling within the bandwidth to −30 dB and corrects the radiation beam tilt to be within −4.5° to 3° from the broadside direction. A gain reduction of 0.6 dB is observed compared to the gain without the slotted decoupling wall.

Introduction

With the development of miniaturization of the present device, decoupling becomes an essential concern in multiple antenna systems, such as in phased array and multi-input-multi-output antennas. Two techniques are generally used for decoupling between patch antennas: (a) change the patch position or shape it and (b) keep the original structure and add a decoupling structure between the patches. In [1], the patches are placed along the diagonal direction to reduce the coupling. In [2], the patches are rotated along the diagonal. In [3], two orthogonal slots on the two adjacent patches were cut along the diagonal and combined with shorting pin to reduce the mutual coupling. However, the most common decoupling technique is the second technique of keeping the original structure and inserting a decoupling structure.

Much work has been presented for decoupling patch antennas where the shape and placement are used. Furthermore, adding a loading structure on top of the patches was used [4–6]. Also, adding a planar structure between the patches was employed [7, 8] as an effective decoupling method. Except these, no additional decoupling techniques were proposed where the weak current distributions are analyzed [9, 10].

However, it was noticed that interference with the decoupling structure causes a tilt for the embedded radiation pattern. This phenomenon exists when a large edge-to-edge distance of over $0.125\lambda_0$ [11–15] exists, where λ_0 is the free space wavelength. Edge-to-edge distance of $0.3\lambda_0$ and $0.25\lambda_0$ in [11] and [12], respectively, had tilted the peak by 10° and 20° at 4.6 GHz. In [13–15], the tilt angles were over 10° for distances around $0.13\lambda_0$. As edges get closer to each other, the mutual coupling gets stronger, and the present decoupling techniques for the closer distances of about $0.05\lambda_0$ show a pattern peak tilt characteristic [16–23]. For a distance greater than $0.05\lambda_0$, the tilt was over 15° [16–20]. The tilt depends on the adopted decoupling methods, which means the tilt angle will not increase as the distance decreases, as the tilt angle was 20° when the distance was $0.077\lambda_0$ [16], while it was 15° with $0.059\lambda_0$ distance [17]. A tilt of 30° for a distance of $0.06\lambda_g$ [18], $0.07\lambda_0$ [19], and $0.057\lambda_0$ [20] was reported, where λ_g is the guided wavelength. A similar property was suited for the separations of less than $0.05\lambda_0$ [21–23]. In [21], the tilt is over 20° for $0.039\lambda_0$ and over 35° for $0.031\lambda_0$ [22] but reduces to about 30° for $0.03\lambda_0$ [23].

Therefore, this study focuses on decoupling techniques with beam tilt correction for edge-to-edge distance of $\lambda_0/20$ along the H-plane. We used a 3D vertical wall to realize a single frequency pattern correction [24] and a realized gain increase using a lower-loss substrate [25]. The present paper proposes a decoupling structure for a beam tilt correction within the whole operating frequency band of interest and a gain reduction of 0.6 dB compared to the no-decoupling case. Here, a 3D vertical wall of FR4 substrate with two-sided cladding is employed, and symmetrical slots on both sides are itched. The vertical conducting walls are connected to the horizontal ground plane of the patch antenna to form a resonant structure and induce reverse current on the wall to reduce the impact of the current generated by the patch. Consequently, the H-plane radiation patterns in the 5.80 GHz band are corrected.

© The Author(s), 2023. Published by Cambridge University Press in association with the European Microwave Association

The rest of the paper is organized as follows. The section "The proposed patch antennas" introduces the whole antenna configuration, including the details of the decoupling wall and the comparisons between the simulations and measurements for verification. Then, the tilt correction is analyzed by forming a resonator in the section "Result analysis." The critical parameters are analyzed to explain their effects on tilt correction and decoupling. The current distributions are compared before and after decoupling. The final section is the conclusion.

The proposed patch antennas

An H-plane arranged two-patch antennas with an edge-to-edge distance of $\lambda_0/20$ is investigated. Then, the 3D metal-slotted vertical wall is inserted between the two patches to reduce the mutual coupling significantly. The details of the proposed technique and the optimized final antenna performance are as follows.

The antennas and decoupling structure

The antennas' detailed configuration with the proposed 3D vertical wall is shown in Fig. 1, where the gray and gold colors represent the dielectric substrate and metal, respectively. The corresponding parameters of the patch antennas and the vertical wall are inserted. Figure 1(a) and (b) show top and side views of the structure, where the negative and the positive indicate the tilt directions from the broadside. The wall is embedded in the substrate and connected to the ground plane. Figure 1(c) indicates that the decoupling structure has three layers, the middle substrate layer and two symmetrical slotted metals. Figure 1(d) shows that the slot is symmetrically etched about the y-axis or the metal. The metal has a proper resonance length to introduce the reverse current from the ground plane, reducing the influence of the current induced on the wall from patch radiation

For the patch antenna design, the substrate F4BTM440 is utilized with a relative dielectric constant of 4.4 and a loss tangent of 0.0033. The conventional patch antenna with a length and width of 46 mm and 31.7 mm, respectively, are used to resonate at 5.80 GHz. Moreover, the quarter-wavelength impedance transformer is applied for impedance matching. Then, another similar patch antenna is placed parallel to the original one along the H-plane, where the edge-to-edge distance is 2.58 mm (about $\lambda_0/20$). After that, the proposed 3D vertical wall is inserted between the patches. Here, the FR4 material is taken as the substrate of the decoupling structure. Its higher dielectric loss will increase the loss of the wall. The relative dielectric constant and loss tangent of the FR4 are 4.4 and 0.025, respectively, and the thickness is 0.8 mm.

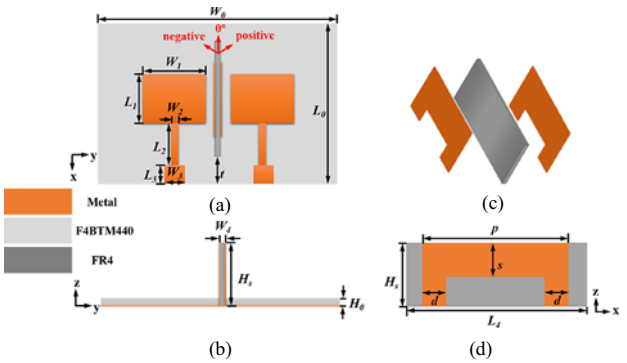


Figure 1. The patches and proposed decoupling structure: (a) top view, (b) side view, (c) exploded view of the vertical wall, and (d) side view of the vertical wall.

Antenna performance

After parametric analysis, we get the final optimized design parameters and results based on the abovementioned method. The corresponding values for the mentioned parameters are listed in Table 1. Photos of the fabricated prototype are shown in Fig. 2. The antenna is measured in the anechoic chamber, as shown in Fig. 3.

The comparisons of the measured and simulated S-parameters are shown in Fig. 4(a). The comparisons show that the measurements agree well with the simulations, though a slight shift of the resonant frequency exists, and the measured S_{21} is lower than that of the simulation. Here, the measured resonant frequency shifts by 50 MHz to 5.85 GHz, and the measured impedance bandwidth

Table 1. Values of antenna parameters

Parameter	Value (mm)	Parameter	Value (mm)	Parameter	Value (mm)
W_0	46	W_3	3	t	3.37
L_0	31.7	L_3	3	p	18.8
W_1	16	W_4	0.8	H_0	1.6
L_1	11.4	L_4	24	H_s	6.5
W_2	0.4	d	2.3		
L_2	6.7	s	3.9		

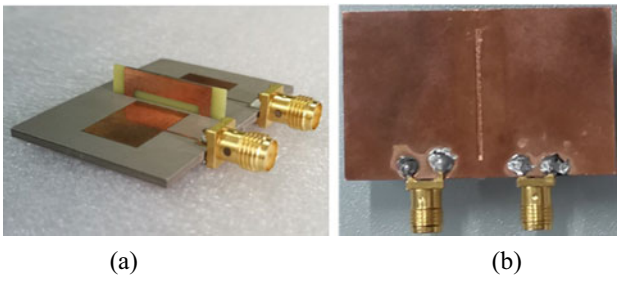


Figure 2. Antenna prototype: (a) 3D view and (b) back view.



Figure 3. Measurement in an anechoic chamber.

https://doi.org/10.1017/S1759078723000752 Published online by Cambridge University Press

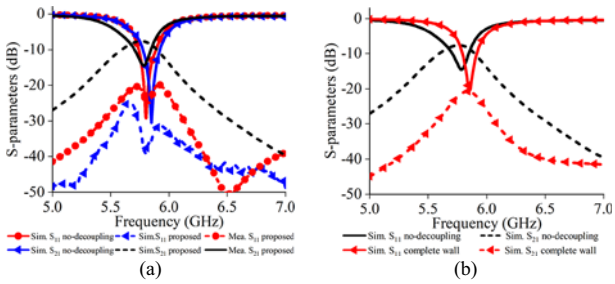


Figure 4. *S*-parameters: (a) with and without decoupling structure and (b) no-decoupling vs. complete wall comparison.

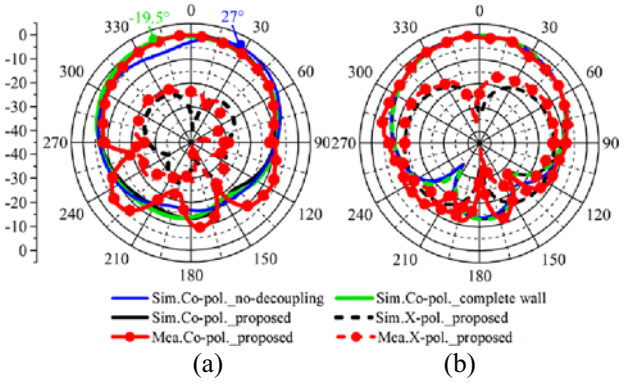


Figure 5. Normalized radiation pattern with and without decoupling structures at the simulated and measured resonance frequencies: (a) H-plane and (b) E-plane.

is 140 MHz from 5.78 to 5.92 GHz, which is 10 MHz less than the simulation. After adding the proposed structure, the isolation becomes better than that without a decoupling structure by 20 dB, which we can judge from the corresponding data of Fig. 4(a), where the measured S_{21} are all below −30 dB in the entire bandwidth while they are over −10 dB of no-decoupling structure. The *S*-parameter comparisons of the no-decoupling structure and the complete wall are shown in Fig. 4(b), which indicates that the complete wall can improve the matching and the isolation if the wall's dimension is proper.

The comparisons of radiation patterns, realized gains, and tilt angles between the simulations and measurements are shown in Figs. 5–7, respectively, where the left antenna of Fig. 1(a) is excited, and the patterns of no-decoupling structure and the complete vertical wall structure are depicted to be compared in Fig. 5. These three comparisons of the proposed structure indicate that the measurements agree well with those of simulations. We only present H-plane patterns because the decoupling arrangement has an insignificant effect on the E-plane patterns.

Figure 5 compares radiation patterns in the E- and H-plane with and without decoupling structure. Each case has a different resonant frequency. The no-decoupling case is considered at 5.78 GHz (simulated) and 5.85 GHz (measured). The proposed decoupling case is presented at 5.80 GHz (simulated) and 5.85 GHz (measured) by black and red lines, respectively. In contrast, the corresponding blue and green lines indicate simulated results of no-decoupling (no wall) and complete wall structures. The H-plane pattern peak direction of the no-decoupling structure is 27°, while it tilts to the other side, −19.5°, when the complete wall is employed, which is corrected to near the broadside direction after using the proposed structure.

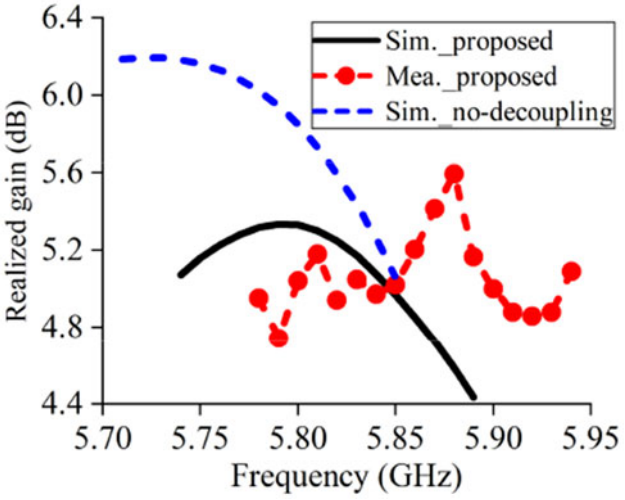


Figure 6. Realized gain comparisons in the bandwidth.

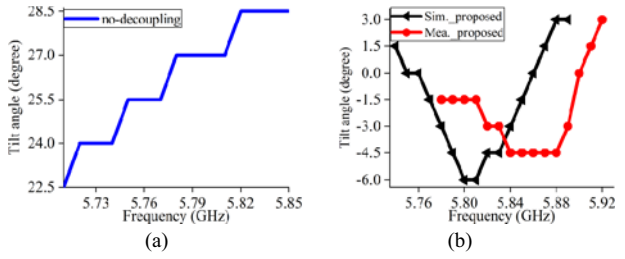


Figure 7. Tilt angle comparisons of H-plane in the bandwidth: (a) without decoupling and (b) with the proposed decoupling structure.

The simulated bandwidth of the proposed structure shifts to a higher band due to the vertical wall, and the measured bandwidth also shifts slightly to a higher level than the simulation. Thus, we show the realized gain of the H-plane in their bandwidth in Fig. 6, where the frequency step is 0.01 GHz. After adding the decoupling structure, the simulated realized gain decreases, and the maximum difference is 0.86 dB. On the contrary, the measured realized gain is higher than the simulation for the proposed structure, but the maximum values appear near the corresponding resonances 5.79 GHz of simulation and 5.88 GHz of measurement, whose difference is 0.25 dB. This difference is because of fabrication error, in which we cannot ensure that the wall is grounded entirely. In addition, the measured result is closer to that with no-decoupling structure with a maximum difference of 0.6 dB.

The tilt angles in the H-plane without decoupling structure are depicted in Fig. 7(a). In the simulated results, the tilts range from 22.5° to 28.5° in the bandwidth with frequency steps of 0.01 GHz. The tilts shown in Fig. 7(b) are reduced to be −6° to 3° range within 5.74 to 5.89 GHz, while the measured show the peak variation within −4.5° to 3° for the bandwidth of 5.78 to 5.92 GHz.

Result analysis

This section analyzes the proposed decoupling structure with the tilt correction by introducing the resonant dimension that induces a correction current on the wall. Then the influences of the main parameters are investigated, and finally, the decoupling effect is presented by the surface current on the patch antenna.

https://doi.org/10.1017/S1759078723000752 Published online by Cambridge University Press

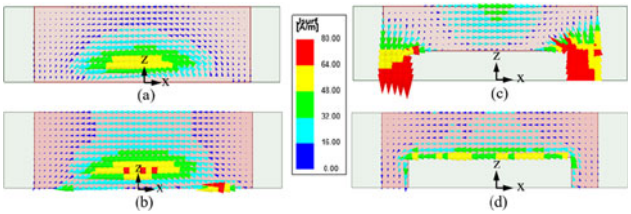


Figure 8. Current distribution comparisons on the vertical wall, (a) grounded whole wall, (b) ungrounded wall, (c) slot in the middle of the wall with grounded ends, and (d) slot with ungrounded ends of the wall.

Tilt correction

As we know, the complete metal wall will play the role of decoupling because it can prevent the direct interference of the excited patch to another. However, the corresponding induced current on the wall affects the radiation performance, the matching, and the realized gain. Thus, we must design the complete wall carefully to get a good matching with the reduction of isolation. Figure 4(b) shows *S*-parameter comparisons of the no-decoupling case with the complete wall decoupling structure. The matching and the isolation are improved after carefully designing the complete wall, while the corresponding H-plane pattern, as shown in Fig. 5(a), tilts in the opposite direction. Because the most concerning problem in this study is the beam direction tilt, we have to modify the wall structure to make the induced current on the wall correct the beam direction rather than deteriorating it. It is found that connecting the wall to the ground, as shown in Fig. 1(b), helps make such a correction.

Exciting the patch antenna induces a current on a fixed area of the complete wall, whether the wall is grounded or not. Figure 8(a) indicates the current distribution for the complete grounded wall case and Fig. 8(b) for the case of the wall shifted up 0.1 mm (ungrounded). The current distributions in both cases are concentrated very close to the ground plane and mainly parallel to it. Thus, this current has an image in the opposite direction, making its broadside contribution very weak and insufficient to correct the beam tilt. A slot is introduced where the current is concentrated to remove the induced current close to the ground. Figure 8(c) shows the current distribution with the slot and grounded ends of the wall. It can be seen that introducing the slot shifts the induced strong current to the wall's outer edges. The top edge, which is further away from the ground plane, acts close to a dipole parallel to the ground and a quarter wavelength from the ground (here, H_s is about $\lambda_0/8$, but because of the dielectric of the substrate and the vertical wall dielectric, it seems that the equivalent electrical length of H_s is close of a quarter of a wavelength), which contributes to the broadside radiation. The side edges act as two out-of-phase monopoles without contributing to the broadside. Thus, the structure radiation is influenced by the slotted vertical wall correcting the beam tilt. If the slotted wall is not grounded, the current distribution concentrates at the upper slot edge, as shown in Fig. 8(d). This current is much closer to the ground plane. Thus, its image current is the opposite, making a feeble contribution to the broadside direction. Thus, the beam tilt is not corrected.

Parameter analysis

All the variables of the vertical wall will affect the matching, decoupling, and pattern tilt of the H-plane. However, the influences of some variables are obvious, such as the height and the width of the wall. So, we pick up two main variables of dimensions d and s to analyze their influences while the size of the metal is fixed and change the loss tangent of the wall substrate to analyze its effect on the *S*-parameters and gain. The height of the protruding part of the wall that is $H_s - H_0$ is 4.9 mm (about 0.21λ, λ is the effective wavelength of FR4), and the width L_4 is 24 mm, about 1.05λ. The total width of the metal on the wall p is 18.8 mm, about 0.82λ. The influences of dimension variables are shown in Fig. 9(a–d), which involve the *S*-parameters and the pattern correction. They almost do not affect the reflection coefficient, except that the variable d has little effect on the resonance frequency and matching, but both affect the decoupling in the bandwidth. These two variables control the size of the slot, which affects the decoupling, but s has a more significant effect. On the contrary, both variables impact the angle of the pattern significantly, that is because they determine the strength of the introduced current (d) or the induced current (s) on the wall. In other words, the final current of the middle part depends on the superposition of the two currents. Figure 9(e) and (f) shows the effect of loss tangent on the antenna performance. This variable affects not only the matching and isolation but also the tilt angle and the realized gain if the size is not changed. This indicates that we should define the corresponding structure parameters for one fixed loss tangent of the wall substrate.

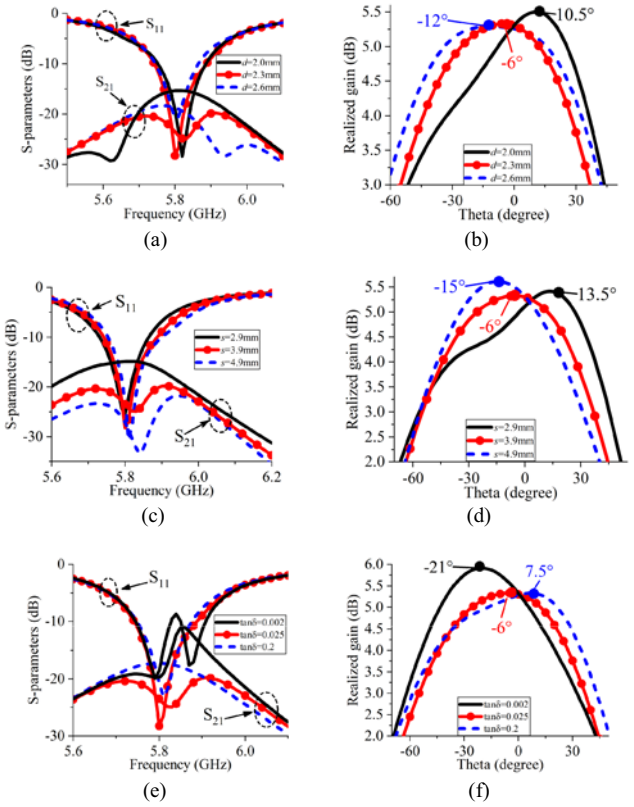


Figure 9. Parameter analysis: (a) *S*-parameter with d, (b) H-plane realized gain at 5.8 GHz with d, (c) *S*-parameter with s, (d) H-plane realized gain at 5.8 GHz with s, (e) *S*-parameters with wall dielectric loss, and (f) 5.8 GHz realized gains of H-plane with wall dielectric loss.

Current distribution on patch

Figure 10 compares current distributions on the two patches at resonances before and after using the proposed structure. The antenna

https://doi.org/10.1017/S1759078723000752 Published online by Cambridge University Press

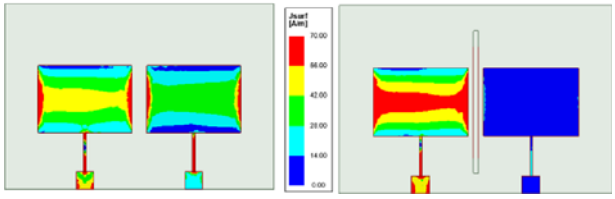


Figure 10. Current distributions on patches at resonances (a) without and (b) with the proposed wall.

on the left is excited, and a matching load terminates the antenna on the right. The coupled current has been suppressed significantly.

Conclusion

The main goal of the present work was to decrease the mutual coupling and correct the beam tilt usually caused by the coupling between the two tightly spaced patches in the H-plane. A vertical wall between the two patches was introduced, reducing the mutual coupling but not correcting the beam tilt. To correct the radiation beam, a slot was introduced on the wall close to the ground plane that perturbed the induced current to influence the radiation characteristics and correct the beam tilt. The proposed structure has been fabricated and measured. After carefully adjusting the corresponding wall parameters, the main beam direction was within the -4.5° to 3° from the broadside direction with a 0.60 dB reduction of the maximum realized gain compared to the simulated one without a decoupling structure. The measurements have agreed well with the simulations.

Financial support. This work was supported by the Natural Science Foundation of Guangxi Province (grant number 2019GXNSFFA245002); the National Natural Science Foundation of China (grant number 12161025 and 62071057); and the Guangxi Key Laboratory of Wireless Wideband Communication and Signal Processing (grant number GXKL06200123 and GXKL06230105).

Competing interests. The authors report no conflict of interest.

References

1. **Zhang YM, Ye QC, Frølund Pedersen G and Zhang S** (2021) A simple decoupling network with filtering response for patch antenna arrays. *IEEE Transactions on Antennas and Propagation* **69**(11), 7427–7439.
2. **Chung KL and Kharkovsky S** (2013) Mutual coupling reduction and gain enhancement using angular offset elements in circularly polarized patch array. *IEEE Antennas and Wireless Propagation Letters* **12**, 1122–1124.
3. **Liu NW, Zhu L, Liu ZX, Li M, Fu G and Liu Y** (2022) A novel low-profile circularly polarized diversity patch antenna with extremely small spacing, reduced size, and low mutual coupling. *IEEE Transactions on Antennas and Propagation* **70**(1), 135–144.
4. **Li M, Zhong BG and Cheung SW** (2019) Isolation enhancement for MIMO patch antennas using near-field resonators as coupling-mode transducers. *IEEE Transactions on Antennas and Propagation* **67**(2), 755–764.
5. **Niu Z, Zhang H, Chen Q and Zhong T** (2019) Isolation enhancement in closely coupled dual-band MIMO patch antennas. *IEEE Antennas and Wireless Propagation Letters* **18**(8), 1686–1690.
6. **Li M, Jiang L and Yeung KL** (2021) Isolation enhancement for MIMO patch antennas sharing a common thick substrate: using a dielectric block to control space-wave coupling to cancel surface-wave coupling. *IEEE Transactions on Antennas and Propagation* **69**(4), 1853–1863.
7. **Alsath MGN, Kanagasabai M and Balasubramanian B** (2013) Implementation of slotted meander-line resonators for isolation enhancement in microstrip patch antenna arrays. *IEEE Antennas and Wireless Propagation Letters* **12**, 15–18.
8. **Yang X, Liu Y, Xu YX and Gong SX** (2017) Isolation enhancement in patch antenna array with fractal UC-EBG structure and cross slot. *IEEE Antennas and Wireless Propagation Letters* **16**, 2175–2178.
9. **Lin H, Chen Q, Ji Y, Yang X, Wang J and Ge L** (2020) Weak-field-based self-decoupling patch antennas. *IEEE Transactions on Antennas and Propagation* **68**(6), 4208–4217.
10. **Lai QX, Pan YM, Zheng SY and Yang WJ** (2021) Mutual coupling reduction in MIMO microstrip patch array using TM_{10} and TM_{02} modes. *IEEE Transactions on Antennas and Propagation* **69**(11), 7562–7571.
11. **Yang F, Peng L, Liao X, Mo K, Jiang X and Li S** (2019) Coupling reduction for a wideband circularly polarized conformal array antenna with a single-negative structure. *IEEE Antennas and Wireless Propagation Letters* **18**(5), 991–995.
12. **Bait-Suwailam MM, Siddiqui OF and Ramahi OM** (2010) Mutual coupling reduction between microstrip patch antennas using slotted-complementary split-ring resonators. *IEEE Antennas and Wireless Propagation Letters* **9**, 876–878.
13. **Wei K, Li J, Wang L, Xing Z and Xu R** (2016) S-shaped periodic defected ground structures to reduce microstrip antenna array mutual coupling. *Electronics Letters* **52**(15), 1288–1290.
14. **Jiao T, Jiang T and Li Y** (2017) A low mutual coupling MIMO antenna using 3-D electromagnetic isolation wall structures. In *IEEE Asia-Pacific Conference on Antennas and Propagation (APCAP)*, 1–2.
15. **Yang XM, Liu XG, Zhou XY and Cui TJ** (2012) Reduction of mutual coupling between closely packed patch antennas using waveguided metamaterials. *IEEE Antennas and Wireless Propagation Letters* **11**, 389–391.
16. **Sun XB and Cao MY** (2017) Low mutual coupling antenna array for WLAN application. *Electronics Letters* **53**(6), 368–370.
17. **Dadashzadeh G, Dadgarpour A, Jolani F and Virdee BS** (2011) Mutual coupling suppression in closely spaced antennas. *IET Microwaves, Antennas & Propagation* **5**(1), 113–125.
18. **Hwangbo S, Yang HY and Yoon YK** (2017) Mutual coupling reduction using micromachined complementary meander-line slots for a patch array antenna. *IEEE Antennas and Wireless Propagation Letters* **16**, 1667–1670.
19. **Lu C, Zhang Q, Qi H, Li S, Zhao H and Yin X** (2019) Compact postwall slotline-based stepped impedance resonator decoupling structure for isolation enhancement of patch antenna array. *IEEE Antennas and Wireless Propagation Letters* **18**(12), 2647–2651.
20. **Gao D, Cao ZX, Fu SD, Quan X and Chen P** (2020) A novel slot-array defected ground structure for decoupling microstrip antenna array. *IEEE Transactions on Antennas and Propagation* **68**(10), 7027–7038.
21. **Habashi A, Nourinia J and Ghobadi C** (2011) Mutual coupling reduction between very closely spaced patch antennas using low-profile folded split-ring resonators (FSRRs). *IEEE Antennas and Wireless Propagation Letters* **10**, 862–865.
22. **OuYang J, Yang F and Wang ZM** (2011) Reducing mutual coupling of closely spaced microstrip MIMO antennas for WLAN application. *IEEE Antennas and Wireless Propagation Letters* **10**, 310–313.
23. **Qi H, Liu L, Yin X, Zhao H and Kulesza WJ** (2016) Mutual coupling suppression between two closely spaced microstrip antennas with an asymmetrical coplanar strip wall. *IEEE Antennas and Wireless Propagation Letters* **15**, 191–194.
24. **Wang Y, Zhang S, Yan Y, Yu X and Kishk AA** (2021) Vertical-wall between tightly spaced patch antennas for decoupling and radiation pattern correction. In *IEEE International Symposium on Antennas and Propagation and USNC-URSI Radio Science Meeting (APS/URSI)*, 1149–1150.
25. **Wang Y, Zhang S, Wang B, Lan D, Yu X, Mo J and Kishk AA** (2022) T-type vertical wall for decoupling and pattern correction of patch antenna. *Applied Sciences* **12**(21), 10732.

https://doi.org/10.1017/S1759078723000752 Published online by Cambridge University Press